Robotica (2015) volume 33, pp. 1113–1130. © Cambridge University Press 2014
doi:10.1017/S0263574714001751

Redundantly actuated 3-RRR spherical parallel manipulator used as a haptic device: improving dexterity and eliminating singularity

Houssem Saafi, Med Amine Laribi* and Said Zeghloul

Department of GMSC, Pprime Institute CNRS, ENSMA, University of Poitiers, UPR 3346, France
E-mail: houssem.saafi@univ-poitiers.fr, said.zeghloul@univ-poitiers.fr

(Accepted June 9, 2014. First published online: July 9, 2014)

SUMMARY
This paper discusses the study of a spherical parallel manipulator (SPM) used as a haptic device for tele-operation applications. The SPM presents poor behavior in singular configurations. Redundancy is used to eliminate the parallel singularity without major changes in the mechanical structure. Comparisons in terms of kinematic and dynamic behavior between the non-redundant and redundant SPM are presented. The results prove the advantage of introducing redundancy in the actuator and sensor to improve the behavior of the SPM. A new control strategy for the redundant SPM is also proposed. The control strategy has been successfully tested and validated on a SimMechanics model.

KEYWORDS: Redundancy; Singularity; Haptic device; Dexterity; Spherical parallel manipulator.

1. Introduction

The use of tele-operation systems in minimally invasive surgery (MIS) has substantially increased in recent years. It has the advantages of being extremely precise, controlled, and a fatigueless process. Human movements are rendered more secure, leading to safer complex surgery operations.

The most known surgery system (da-Vinci), which is a multi-application system, is expensive and cumbersome (a large room is needed to contain all the parts of the system).[1] The aim of our current research is not to develop an autonomous system, but to develop a special application for cheap and portable systems.[2]

A newly developed spherical parallel manipulator (SPM) is presented in this paper as a haptic device for a tele-operation system for medical applications. The developed device should provide the surgeon with more dexterity, accuracy, and force feedback during tele-operation.

However, parallel manipulators suffer from parallel singularities which generate large actuator torques or forces, and a loss of stiffness. In singular configurations a manipulator loses one or more of its degrees of freedom (d.o.f.s). Most works try to eliminate this type of singularity from the workspace of the robot by optimizing its geometry.[3,4] However, by improving the kinematic behavior, the parallel robot structure becomes larger and a problem of interference is generated.[5] In this paper, the singularity of SPM is investigated and a solution based on redundancy is proposed and developed to overcome its effect. Redundancy can be used for both force control[6] and motion control[7,8] in order to improve the kinematic and dynamic performances of both serial and parallel manipulators. To improve control performances, redundant sensors (extra sensors) can be used.[9] In the present work an extra sensor is used to simplify the Forward Kinematic Model (FKM) and to speed up the calculation time.

The paper is organized as follows. In Section 2, the identification of the workspace, based on the capture of gestures of a medical expert performing a MIS, is shown. In Section 3, the SPM singularities and the dexterity distribution are analyzed and reported. The redundant actuation is introduced to eliminate singularity and to improve dexterity in Section 4. A comparison of the non-redundant and

* Corresponding author. E-mail: med.amine.laribi@univ-poitiers.fr

https://doi.org/10.1017/S0263574714001751 Published online by Cambridge University Press

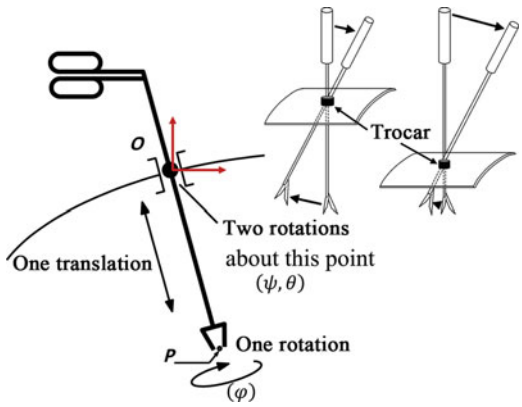


Fig. 1. MIS possible movement.

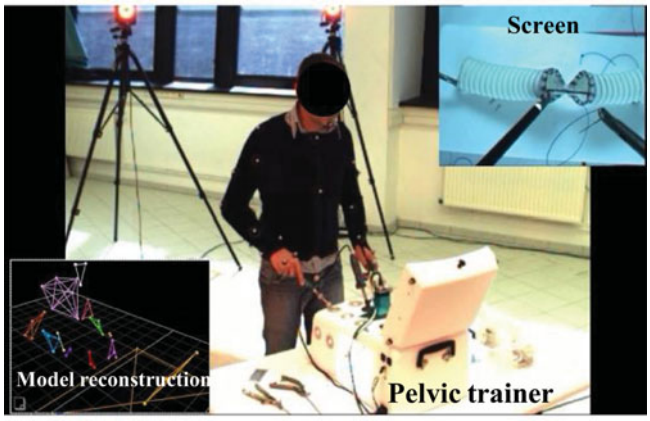


Fig. 2. Experimental setup (pelvic trainer) and motion reconstitution of the suturing operation.

redundant actuated SPM is carried out. Section 5 deals with the control strategy of the redundant SPM. Finally, Section 6 summarizes this paper.

2. Workspace Identification of the Minimally Invasive Surgery

Minimally invasive surgery is a new trend in surgery practice. Through the use of tiny incisions, faster recovery can be achieved due to MIS compared with general surgery. Currently there is a strong interest in the development of this technology. The first robotic human surgery with single port, using Da Vinci platform, was performed only recently.[10]

In MIS the instruments are designed to enter the patient's body through a tiny incision using a trocar, see Fig. 1.

Minimally invasive surgery robots need a large workspace. The issue of the workspace size has been reported by Thakre.[11] For instance, for the da Vinci robot system, it has been established that no task could be performed in a 40-mm edge cube due to collisions between arms. Besides, a small workspace prevents optimal surgical functioning.

The possible motions of the instruments are three rotations around the incision point and one translation along the axis of the instrument. In this work, the rotations are described by the three ZXZ Euler angles (ψ, θ, and φ) as presented in Fig. 1.

In order to identify the needed workspace, the movements of the surgeon are recorded with equipment dedicated to laparoscopy learning techniques: the pelvic-trainer, see Fig. 2.

A vicon motion capture system was used to record the trajectories of markers placed on the tools. The intended application is suture end-to-end anastomosis, which consists of suturing two parts of a ruptured hollow organ. Two tools are used by the expert: a clamp and a needle holder.[12]

https://doi.org/10.1017/S0263574714001751 Published online by Cambridge University Press

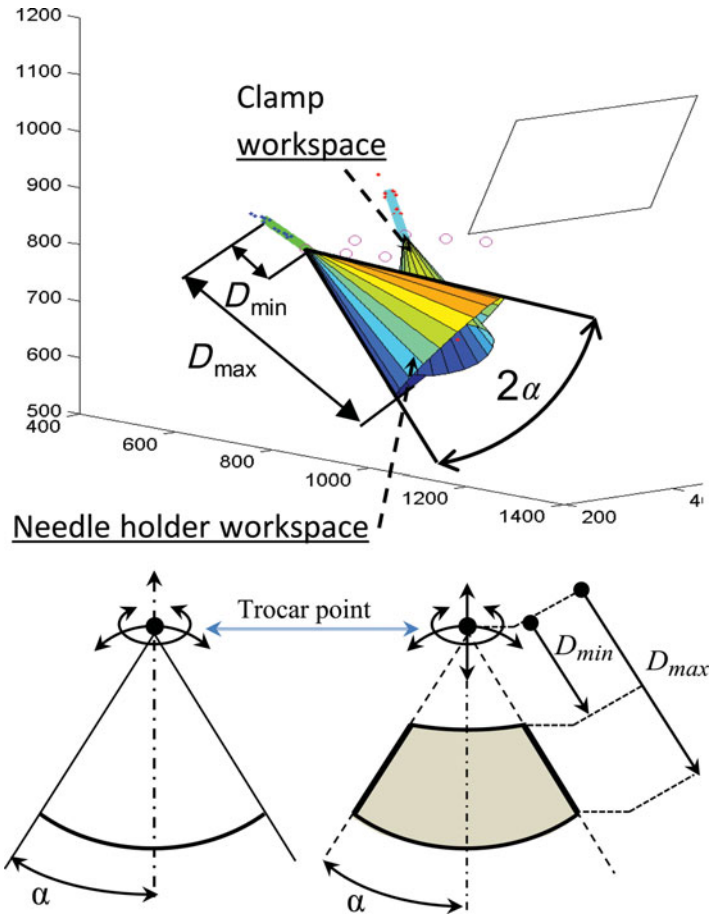


Fig. 3. The needed workspace for MIS tool.

The obtained data were used to evaluate the size of the workspace within which the tools were moving. The cone with a half apex angle, α, is used to evaluate the workspace size generated by the axis of each tool.

A cone is represented for each tool (see Fig. 3). These cones include the workspace required for all the performed tasks. The first corresponds to the clamp with an apex angle of 17° and the second to the needle holder with an apex angle of 26°.

Besides the rotations, each tool has also a translation motion along the axis of the cone defined by the maximum and minimum distances, respectively ($D_{\max}$) and ($D_{\min}$). This represents the distance between the point of incision and the tool tip.

The self-rotation φ must be more than $\pm 90°$. In the (ψ, θ) plane, the workspace of the suture application is represented by a pseudo-circular shape. Figure 4 shows the workspace and the captured orientations of the tool in the plane (ψ, θ).

From these results, it is clear that the most useful area of the workspace is at the center. Within this region, the developed haptic device must offer large kinematic performances as well as a uniform behavior. The evaluation criteria used in this work are based on the kinematic performances of the manipulator.

In the next section, the kinematic performances of the manipulator are evaluated and enhanced.

3. Evaluation of the Spherical Parallel Manipulator

The proposed haptic device is a SPM. This choice is motivated mainly by the fact that the output motions of this type of mechanism are three rotations around a fixed center of rotation (CoR). This makes the SPM a natural and suitable candidate for the MIS application. Typically, the surgical robotic arm for MIS application should have a remote center of motion. This center can be defined as

https://doi.org/10.1017/S0263574714001751 Published online by Cambridge University Press

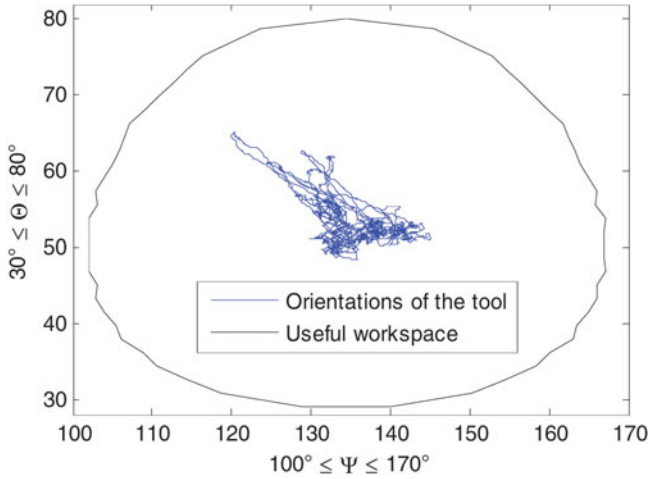


Fig. 4. Useful area of the workspace.

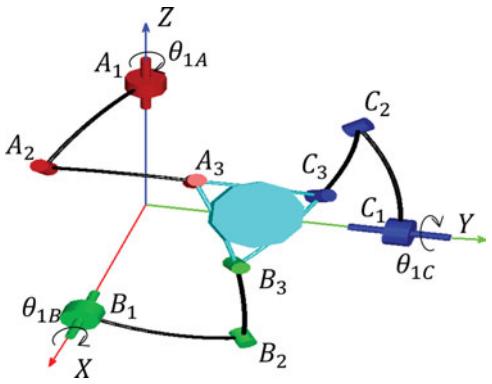


Fig. 5. Spherical parallel manipulator.

a fixed point outside the mechanism. Second, the SPM haptic device has the advantage of the parallel structures in terms of rigidity and accuracy. Moreover, for parallel architectures, motors are fixed on the base. This reduces the torques applied by the motors to overcome the gravity of the mechanism and leads to smaller motors.

3.1. Kinematic model

The SPM is a robot with 3 rotation d.o.f.s (see Fig. 5). These rotations are represented by the ZXZ Euler angles ψ, θ, and φ. Each leg of the SPM is made of two links and three revolute joints. All the axes of the revolute joints are intersecting at one point, called the center of the robot. This point coincides with a remote center of motion. Each link is characterized by the angle between its two revolute joints, e.g. see Fig. 6. This angle is constant and it represents the dimension of the link.

The three revolute joints located on the base are actuated. The three legs are identical and the actuated joint axes are along the three orthogonal axes X, Y, and Z, respectively.

In the previous works,[13,14] the optimal geometric parameters of SPM were defined. A multi-objective optimization procedure based on a genetic algorithm method was carried out to identify the optimal SPM. Two criteria, related to the SPM workspace and kinematic dexterity, were considered. The identified workspace can be represented by a cone with a half apex angle of 26°, as presented in Section 2. After optimization, the resulting geometry is described by $[\alpha,\ \beta,\ \gamma] = [39.3°,\ 34.1°,\ 18.2°]$.

For parallel robots, the Jacobian matrix is composed of two matrices: parallel matrix **A** and serial matrix **B**, see Eq. (1).

$$\mathbf{A}\omega = \mathbf{B}\dot{\theta}. \tag{1}$$

https://doi.org/10.1017/S0263574714001751 Published online by Cambridge University Press

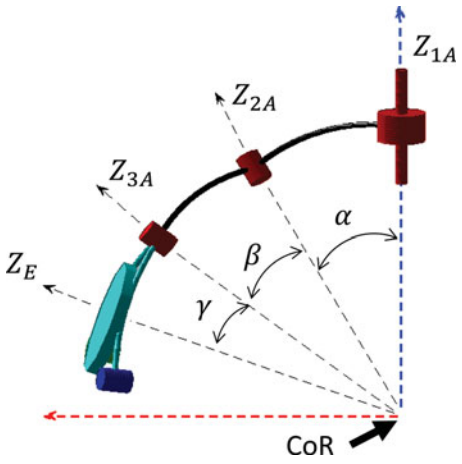


Fig. 6. Parameters of leg A.

For a fully-parallel manipulator, the matrix **B** is a diagonal matrix and its inverse is obtained immediately. Therefore, we propose the use of the inverse Jacobian matrix in the input/output velocity relation as follows:

$$\dot{\theta} = \mathbf{J}^{-1}\omega, \tag{2}$$

with

$$\mathbf{J}^{-1} = \mathbf{B}^{-1}\mathbf{A}. \tag{3}$$

ω is the angular velocity of the end effector expressed as follows:

$$\omega = \begin{bmatrix} \dot{\theta}\cos(\psi) + \dot{\varphi}\sin(\theta)\sin(\psi) \\ \dot{\theta}\sin(\psi) - \dot{\varphi}\sin(\theta)\cos(\psi) \\ \dot{\psi} + \cos(\theta) \end{bmatrix}. \tag{4}$$

The matrices **A** and **B** can be expressed by differentiating the geometric Eq. (5). For the leg k (k = A, B, C), we can write

$$\mathbf{Z_{2k}} \cdot \mathbf{Z_{3k}} = \mathbf{cos}\beta. \tag{5}$$

The obtained equation can be written as:

$$\dot{\mathbf{Z}}_{\mathbf{2k}} \cdot \mathbf{Z_{3k}} + \mathbf{Z_{2k}} \cdot \dot{\mathbf{Z}}_{\mathbf{3k}} = 0, \tag{6}$$

with

$$\dot{\mathbf{Z}}_{\mathbf{2k}} = \dot{\theta}_{\mathbf{1k}}\mathbf{Z_{1k}} \times \mathbf{Z_{2k}}, \tag{7}$$

$$\dot{\mathbf{Z}}_{\mathbf{3k}} = \omega \times \mathbf{Z_{3k}}, \tag{8}$$

Replacing these expressions in Eq. (6), we get

$$(\mathbf{Z_{1k}} \times \mathbf{Z_{2k}} \cdot \mathbf{Z_{3k}}) \cdot \dot{\theta}_{\mathbf{1k}} = \mathbf{Z_{3k}} \times \mathbf{Z_{2k}} \cdot \omega. \tag{9}$$

So, matrix **A** is a 3 × 3 matrix and it is defined as follows:

$$\mathbf{A} = \begin{bmatrix} \mathbf{Z_{3A}} \times \mathbf{Z_{2A}} & \mathbf{Z_{3B}} \times \mathbf{Z_{2B}} & \mathbf{Z_{3C}} \times \mathbf{Z_{2C}} \end{bmatrix}^{\mathbf{T}}. \tag{10}$$

https://doi.org/10.1017/S0263574714001751 Published online by Cambridge University Press

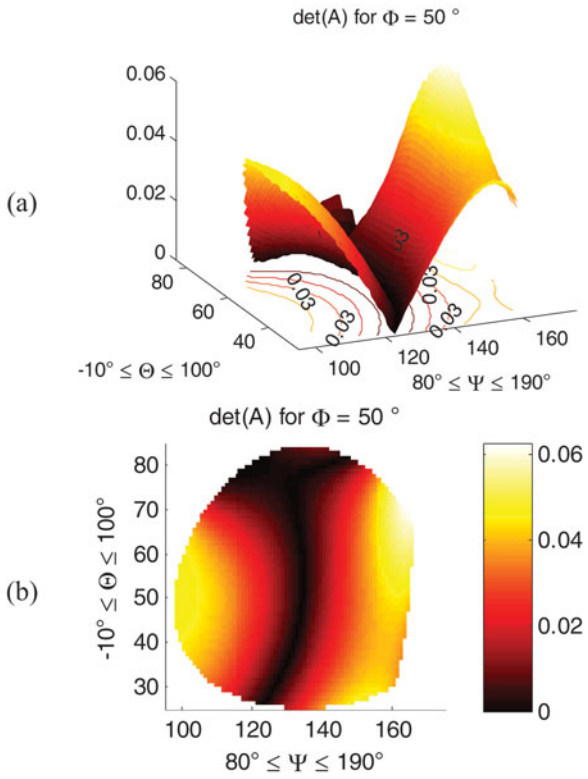


Fig. 7. Determinant of matrix A (singularities area in black).

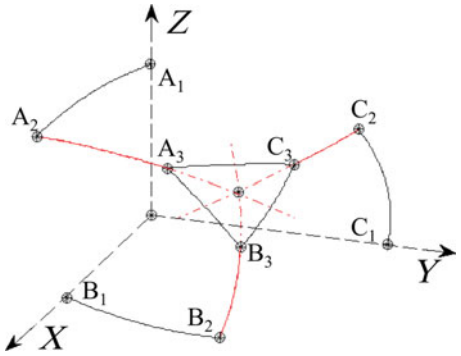


Fig. 8. Parallel singularity: central configuration.

Matrix **B** is a diagonal 3×3 matrix and it is defined as follows:

$$\mathbf{B} = \operatorname{diag}[\mathbf{Z}_{1A}(\mathbf{Z}_{2A} \times \mathbf{Z}_{3A}) \quad \ldots \quad \mathbf{Z}_{1B}(\mathbf{Z}_{2B} \times \mathbf{Z}_{3B}) \quad \mathbf{Z}_{1c}(\mathbf{Z}_{2c} \times \mathbf{Z}_{3c})] \,. \tag{11}$$

3.2. Presence of singularity

The major limitation of the SPM structure is the presence of parallel singularity called type-II singularity inside the useful workspace. For $\varphi = 50°$, the singularity is in the center of the workspace. The distribution of the determinant of matrix **A** is presented in Fig. 7.

The parallel singularity occurs when the three segments connected to the effector k_2k_3 intersect for $k =$ A, B or C, e.g. see Fig. 8. In these configurations, the determinant of parallel matrix A vanishes.

The first effect of the parallel singularity is the amplification of error in the kinematic transformations between joint and Cartesian spaces. The second effect is the amplification of the

https://doi.org/10.1017/S0263574714001751 Published online by Cambridge University Press

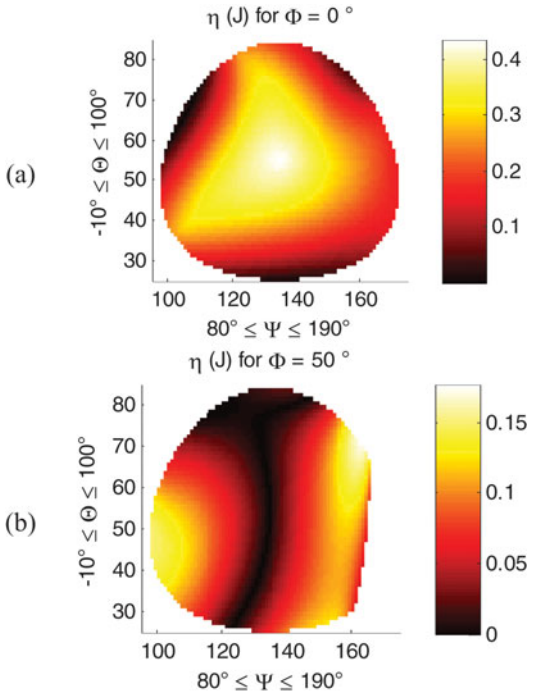


Fig. 9. Dexterity distribution for: (a) $\varphi = 0^\circ$; (b) $\varphi = 50^\circ$.

actuated joint torques. The singularity leads to the elimination of 1 d.o.f. Hence, the self-rotation becomes uncontrollable in singular configurations.

3.3. Dexterity

To evaluate the kinematic performances of robots, several criteria were introduced. Dexterity is a measure that indicates the ability of a robot to perform motions around a point of its workspace. It can also measure how far the end-effector from the singular configurations is. In the literature, several methods are proposed to compute the dexterity of a given structure. Here, we have chosen the most used method, which is based on the condition number $\kappa(\mathbf{J})$ of the Jacobian matrix $\mathbf{J}$.[15,16] For a given design vector $[\alpha, \beta, \gamma]$, the local dexterity at the orientation $[\psi, \theta, \varphi]$ is

$$\kappa(\mathbf{J}) = ||\mathbf{J}|| \cdot ||\mathbf{J}^{-1}||. \tag{12}$$

Let $\eta_{\mathbf{J}}$ represent the inverse of the condition number $\kappa(\mathbf{J})$. Figure 9 shows the local dexterity distribution for a self-rotation at 0° and 50°.

We can observe that for $\varphi = 0^\circ$, local dexterity is maximum in the center of the workspace. For $\varphi = 50^\circ$, local dexterity is minimum in the center. This constitutes a major drawback since the center of the workspace is an important region for MIS application.

In the next section, we propose a solution to improve the dexterity of the SPM. The proposed solution also eliminates the singularity.

4. Redundant 3-RRR SPM and Dexterity Improvement

To remove singularity and improve dexterity, we propose to add a redundant actuator on the joint of the axis $\mathbf{Z}_{3A}$, as illustrated in Fig. 10.

In the case of redundant SPM, the dimension of the joint velocities vector θ increases:

$$\dot{\theta} = \begin{bmatrix} \dot{\boldsymbol{\theta}}_{1A} & \dot{\boldsymbol{\theta}}_{1B} & \dot{\boldsymbol{\theta}}_{1C} & \dot{\boldsymbol{\theta}}_{3A} \end{bmatrix}^{\mathbf{T}}. \tag{13}$$

https://doi.org/10.1017/S0263574714001751 Published online by Cambridge University Press

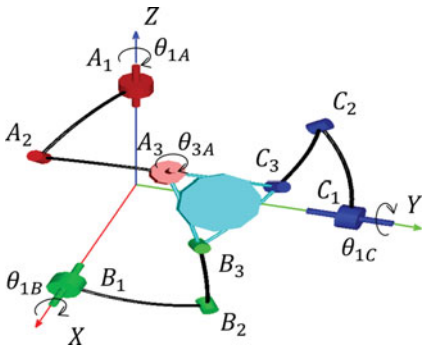


Fig. 10. Redundant spherical parallel manipulator.

The kinematic model of this redundant manipulator can be expressed as follows:

$$\mathbf{A}_r\omega = \mathbf{B}_r \begin{bmatrix} \dot{\theta}_{1A} \\ \dot{\theta}_{1C} \\ \dot{\theta}_{1C} \\ \dot{\theta}_{3A} \end{bmatrix}. \tag{14}$$

Consequently, we detail the Jacobian matrix of the redundant SPM. The angular velocity of the platform, ω, is defined as a function of the angular velocities of the joints. If we consider the leg A, the angular velocity of the platform can be expressed as follows:

$$\omega = \dot{\theta}_{1\mathbf{A}} \cdot \mathbf{Z}_{1\mathbf{A}} + \dot{\theta}_{2\mathbf{A}} \cdot \mathbf{Z}_{2\mathbf{A}} + \dot{\theta}_{3\mathbf{A}} \cdot \mathbf{Z}_{3\mathbf{A}}. \tag{15}$$

To eliminate the passive angular velocity $\dot{\theta}_{2A}$ and the active angular velocity $\dot{\theta}_{1A}$, we use the reciprocal screw theory method. We multiply Eq. (15) by a reciprocal vector $\mathbf{V}^r_{3A}$ to $\mathbf{Z}_{1A}$ and $\mathbf{Z}_{2A}$, and not to $\mathbf{Z}_{3A}$. This vector is perpendicular to the plane spanned by $\mathbf{Z}_{1A}$ and $\mathbf{Z}_{2A}$. The vector $\mathbf{V}^r_{3A}$ can be expressed as follows:

$$\mathbf{V}^{\mathbf{r}}_{3\mathbf{A}} = \mathbf{Z}_{1\mathbf{A}} \times \mathbf{Z}_{2\mathbf{A}}. \tag{16}$$

So the expression (15) becomes:

$$\mathbf{V}^{\mathbf{r}}_{3\mathbf{A}} \cdot \omega = \dot{\theta}_{3\mathbf{A}} \cdot \mathbf{V}^{\mathbf{r}}_{3\mathbf{A}} \cdot \mathbf{Z}_{3\mathbf{A}}, \tag{17}$$

$$(\mathbf{Z}_{1\mathbf{A}} \times \mathbf{Z}_{2\mathbf{A}}) \cdot \omega = \dot{\theta}_{3\mathbf{A}} \cdot (\mathbf{Z}_{1\mathbf{A}} \times \mathbf{Z}_{2\mathbf{A}}) \cdot \mathbf{Z}_{3\mathbf{A}}. \tag{18}$$

The serial matrix $\mathbf{B}_r$, for the redundant SPM, becomes a 4×4 orthogonal one and the parallel matrix $\mathbf{A}_r$ becomes a 4×3 matrix defined as follows:

$$\boldsymbol{A}_r = \begin{bmatrix} \mathbf{Z}_{2A} \times \mathbf{Z}_{3A} & \mathbf{Z}_{2B} \times \mathbf{Z}_{3B} & \mathbf{Z}_{2c} \times \mathbf{Z}_{3c} & \mathbf{Z}_{1A} \times \mathbf{Z}_{2A} \end{bmatrix}^{\mathbf{T}}, \tag{19}$$

$$\boldsymbol{B}_r = \mathbf{diag}[\mathbf{Z}_{1A}(\mathbf{Z}_{2A} \times \mathbf{Z}_{3A}) \quad \mathbf{Z}_{1B}(\mathbf{Z}_{2B} \times \mathbf{Z}_{3B}) \quad \ldots \mathbf{Z}_{1c}(\mathbf{Z}_{2c} \times \mathbf{Z}_{3c}) \quad \mathbf{Z}_{3A}(\mathbf{Z}_{1A} \times \mathbf{Z}_{2A})]. \tag{20}$$

The inverse of the Jacobian matrix ($\mathbf{J}_r^{-1} = \mathbf{B}_r^{-1}\mathbf{A}_r$) becomes a 4×3 non-square matrix. To evaluate the presence of parallel singularities the determinant of matrix $\mathbf{A}_r$, Δ_r, is needed. For non-square matrices, we use the following expression in order to evaluate singularities:

$$\Delta_{\mathbf{r}} = \mathbf{det}\left(\mathbf{A}_r^{\mathbf{T}} \cdot \mathbf{A}_r\right). \tag{21}$$

Figure 11 shows the distribution of the determinant Δ_r of the redundant SPM for $\varphi = 50^\circ$.

Due to the redundancy, the determinant Δ_r does not vanish for the whole useful workspace. The parallel singularity is thus eliminated.

https://doi.org/10.1017/S0263574714001751 Published online by Cambridge University Press

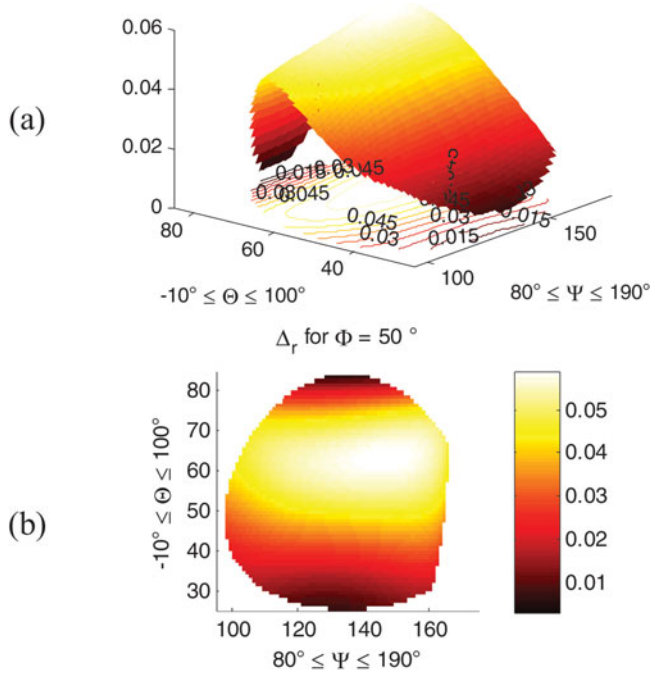


Fig. 11. Determinant Δ_r for the redundant SPM.

Figure 12 shows, that for $\varphi = 0^\circ$ and $\varphi = 50^\circ$, the maximum value of the local dexterity is reached at the center of the workspace. The dexterity of the SPM for $\varphi = 50^\circ$ has been highly improved without major design changes.

In order to evaluate and compare the dexterity distribution for all the configurations inside the workspace, we propose to use the global dexterity index **GDI**. This dexterity index consists of integrating the dexterity over the workspace and then normalizing it by the volume of the workspace. This leads to

$$\mathbf{GDI} = \frac{\int_v \eta_J \mathbf{d}v}{\int_v \mathbf{d}v}, \tag{22}$$

where η_J is the local dexterity for a given configuration and dv represents the volume element of the workspace v. To calculate this value numerically the workspace was discretized in N nodes for each value of the self-rotation φ.

$$\mathbf{GDI} \approx \frac{1}{N} \sum_{i=1}^{N} \eta_{J_i}. \tag{23}$$

Figure 13 shows the evolution of the GDI according to the self-rotation φ.

One can observe that the dexterity of the robot has been improved for the whole range of self-rotation.

The dexterity could be further improved by optimizing the redundant SPM.[17] There are many criteria other than dexterity which can be considered, for example, stiffness and workspace.[18,19] The force and motion controls could benefit from enhancing the kinematic performances of the optimal redundant robot.

5. Control Strategy for the Redundant SPM

The SPM is used as a haptic device to control a surgery robot and to provide the feedback of efforts generated by the interaction between the tools and the patient's body.

https://doi.org/10.1017/S0263574714001751 Published online by Cambridge University Press

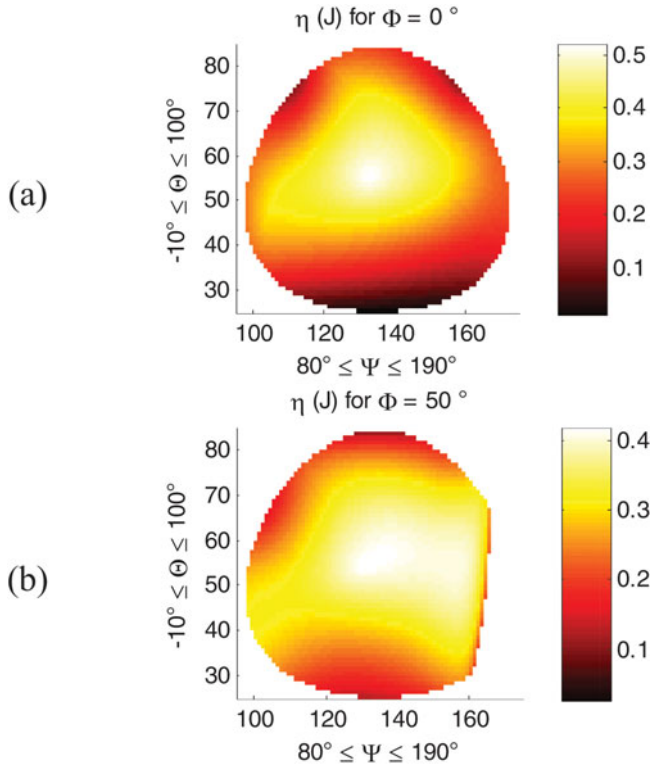


Fig. 12. Dexterity distribution for: (a) $\varphi = 0°$; (b) $\varphi = 50°$.

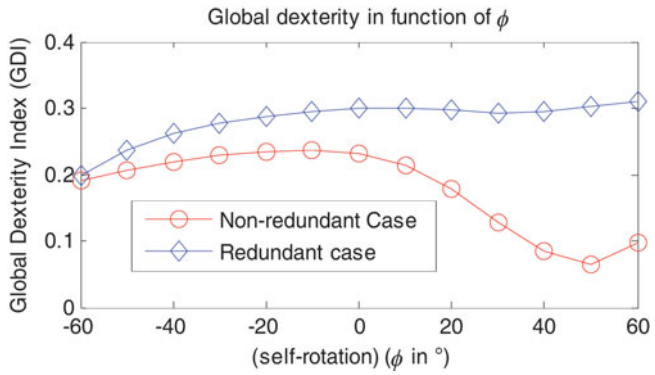


Fig. 13. Global dexterity index: comparison between the redundant and non-redundant SPMs.

The orientation of the haptic device is obtained by solving the FKM of the SPM for a given configuration of the actuated joints. Section 5.1 focuses on the FKM of the redundant SPM. The force feedback control strategy is presented in Section 5.2.

5.1. Forward Kinematic Model of the SPM with redundant sensor

Solving the FKM of parallel manipulators is a complex task.[20–22] In the case of the SPM, the direct model calculates the orientation of the platform given by Euler angles (ψ, θ, and φ) for a given configuration of the actuated joints ($\theta_{1A}, \theta_{1B}, \theta_{1C}$). Only three sensors are needed to define the FKM, but near the singularity, the accuracy of the FKM solution does not meet the control requirement. Also, by using three sensors, the calculation time is longer than 100 ms, which is not appropriate for real-time applications. Here, we propose to add a redundant sensor to improve the accuracy and to speed up the calculation time.

https://doi.org/10.1017/S0263574714001751 Published online by Cambridge University Press

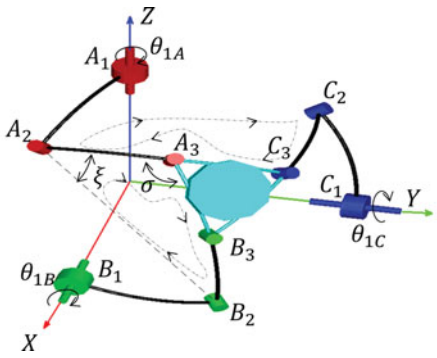


Fig. 14. The considered four-bar spherical mechanisms in SPM: A2-A3-B3-B2 and A3-A2-C2-C3.

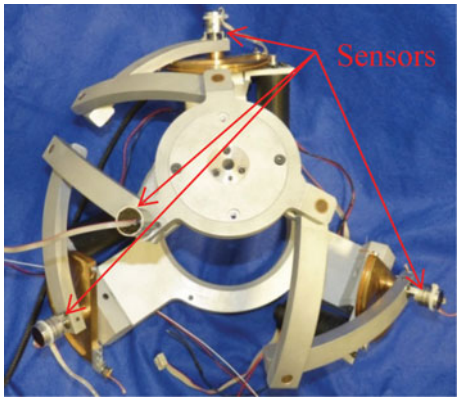


Fig. 15. The developed SPM with four sensors.

Several studies have led to the resolution of the forward kinematic of the SPM.[23–25] The FKM studied by Gosselin *et al.*[24] is represented by an eighth-order polynomial and has eight possible solutions. An alternative to the traditional algebraic approaches to find the solutions of the FKM of parallel manipulators consists of using interval methods.[23] A typical problem of this method is its sensitivity to the size of the initial intervals. Bai *et al.*[25] proposed a robust procedure to determine the platform orientation by using the input/output equations of spherical four-bar linkages. In this paper an approach similar to that used in ref. [25] is used.

The two considered four-bar spherical mechanisms are described by the following two chains: A2-A3-B3-B2 and A3-A2-C2-C3, and are represented in Fig. 14.

The corresponding input/output equations can be written as follows:

For the chain A2-A3-B3-B2 the equation is

$$\mathbf{L}_1 \cos(\xi) + \mathbf{M}_1 \sin(\xi) + \mathbf{N}_1 = 0. \tag{24}$$

For the chain A3-A2-C2-C3 the equation is

$$\mathbf{L}_2 \cos(\xi) + \mathbf{M}_2 \sin(\xi) + \mathbf{N}_2 = 0, \tag{25}$$

where ξ is the angle (A3A2B2), σ is the angle (A2A3B3), and $\mathrm{L}_i(\sigma)$, $\mathrm{M}_i(\sigma)$, $\mathrm{N}_i(\sigma)$ $(i = 1, 2)$ are coefficients that depend on $\cos(\sigma)$ and $\sin(\sigma)$.

The unknowns of the system composed of Eqs. (24) and (25) are ξ and σ. The angle σ is given directly by the fourth sensor located on the $\mathbf{Z}_{3A}$ axis, see Fig. 15. The fourth sensor reduces the complexity of the system and makes it simple to solve.

https://doi.org/10.1017/S0263574714001751 Published online by Cambridge University Press

From the system composed of Eqs. (24) and (25), $\cos\xi$ and $\sin\xi$ can be expressed as follows:

$$\begin{cases} \cos(\xi) = \frac{\mathbf{M_1N_2 - M_2N_1}}{\mathbf{L_1M_2 - L_2M_1}} & : (\mathbf{a}) \\ \sin(\xi) = -\frac{\mathbf{L_1N_2 - L_2N_1}}{\mathbf{L_1M_2 - L_2M_1}} & : (\mathbf{b}) \end{cases}, \tag{26}$$

with $\mathbf{L_1M_2} - \mathbf{L_2M_1} \neq 0$ for all configurations in the workspace.

The unique solution of ξ is defined by

$$\xi = \mathbf{atan}\,2(\sin\xi, \cos\xi). \tag{27}$$

The platform orientation can be calculated using the direct kinematic of leg A. This is defined by the transformation matrix expressed as follows:

$$\mathbf{T}_0^3\big|_{\mathbf{A}} = \mathbf{Rot}(\mathbf{Z}, \theta_{1\mathbf{A}}) \cdot \mathbf{Rot}(\mathbf{X}_{1\mathbf{A}}, \alpha) \cdot \mathbf{Rot}(\mathbf{Z}_{2\mathbf{A}}, \xi) \cdot \mathbf{Rot}(\mathbf{X}_{2\mathbf{A}}, \beta) \cdot \mathbf{Rot}(\mathbf{Z}_{3\mathbf{A}}, \sigma) \cdot \mathbf{Rot}(\mathbf{X}_{3\mathbf{A}}, \gamma). \tag{28}$$

The orientation of the platform can also be expressed using Euler ZXZ transformation:

$$\mathbf{T}_0^3\big|_{\mathbf{A}} = \mathbf{Rot}(\mathbf{Z}, \psi) \cdot \mathbf{Rot}(\mathbf{X}', \theta) \cdot \mathbf{Rot}(\mathbf{Z}'', \varphi). \tag{29}$$

The Euler angles ψ, θ, and ϕ can be calculated from Eqs. (28) and (29).

The use of the fourth sensor reduces the number of unknowns. The FKM resolution becomes simple since the value of σ is given by the sensor. This redundant sensor speeds up the resolution of the FKM and leads to a running time less than 16 μs.[26]

5.2. Force-feedback control strategy for the redundant SPM

Let $\mathbf{T}$ denote the torque applied by the haptic device to the user and τ the torque vector provided by the actuators. One can write,

$$\tau = \mathbf{J^T T} + \tau_{\mathbf{s}} + \tau_{\mathbf{d}}, \tag{30}$$

where $\mathbf{J}^{\mathrm{T}}$ is the transpose of the Jacobian matrix, τ_d is the torque provided by the actuators to overcome the dynamic behavior of the haptic device. Also, τ_{s} is the torque provided by the actuators to overcome the gravity effort applied on the haptic device.

The dynamic behavior of the haptic device is neglected since the speed and acceleration level are low.

The static torque, $\tau_{\mathbf{s}}$, is calculated by solving the static equilibrium model of the SPM. The 3-RRR SPM is an over-constraint system. So the equilibrium is written for an equivalent and non-over-constraint SPM, which is 3-RRS (S as spherical joint and R as revolute joint).[27]

In singularity-free configuration, the components of vector τ are always lower than the maximum torque of the actuators, $\tau_{\max}$. However, in singular configurations τ exceeds $\tau_{\max}$, see Fig. 21.

As has been shown in the previous section, the redundancy overcomes the problem of the presence of singularities. On the other hand, the Jacobian matrix of the redundant SPM is non-square. This complicates the haptic control due to the real-time constraint.

In order to simplify the control of the redundant SPM, we propose that the added actuator on the axis $\mathbf{Z}_{3A}$ replace the actuator defined by the axis $\mathbf{Z}_{1A}$, when the end-effector is in a singular configuration. This means that two cases are identified for this approach: a singularity-free mode, noted by mode 1, and a singular mode, noted by mode 2. As a result for each mode a non-redundant structure is to be considered.

To examine which configuration is singular or close to the singular configuration, either the smallest singular value[28] or the limit of the actuated joint torques can be used. In our approach, the joint torque limit is used to check whether the end-effector enters into a singular region. When τ reaches 90% of $\tau_{\max}$, we consider that the end-effector is close to a singular configuration.

https://doi.org/10.1017/S0263574714001751 Published online by Cambridge University Press

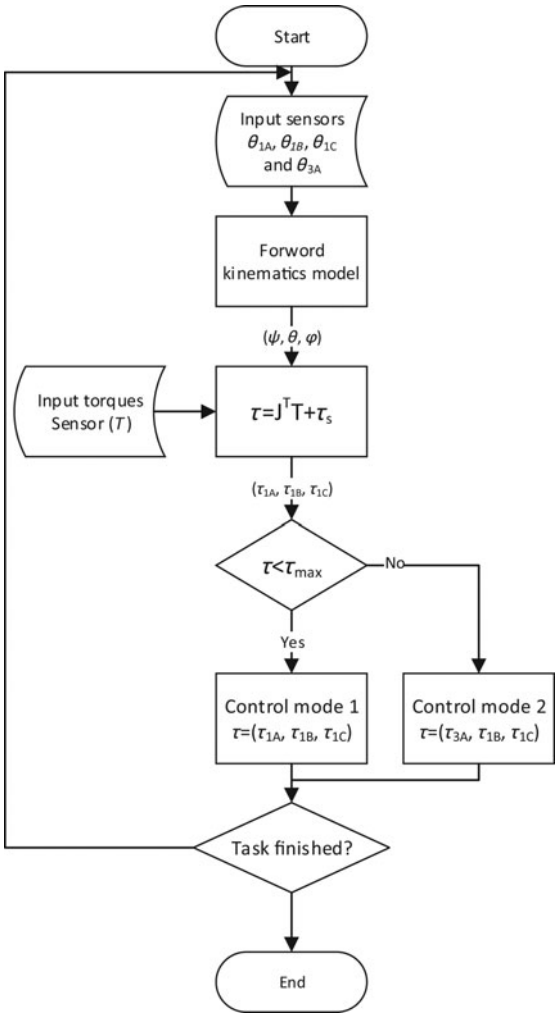


Fig. 16. The switching mode algorithm.

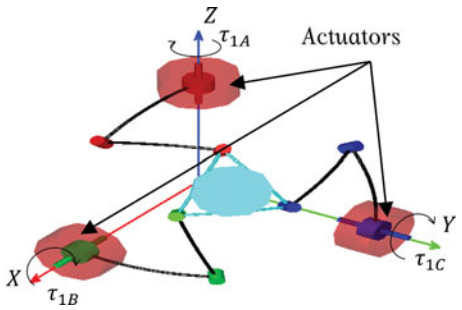


Fig. 17. Control mode 1 for singularity-free configurations.

The joint torques taken into account are τ_{1A}, τ_{1B}, and τ_{1C}. The end-effector is considered to be in a singular region if any joint torque exceeds its limit. The algorithm that handles the control switching mode is presented in Fig. 16.

1. Control mode 1
   The conventional control corresponds to the non-singular configuration. In this case, the actuators on the axes $\mathbf{Z}_{1A}$, $\mathbf{Z}_{1B}$, and $\mathbf{Z}_{1C}$ are active while the fourth actuator on the axis $\mathbf{Z}_{3A}$ becomes passive. The SPM is equivalent to the one in Fig. 17. The provided torque vector, τ, is equal to

https://doi.org/10.1017/S0263574714001751 Published online by Cambridge University Press

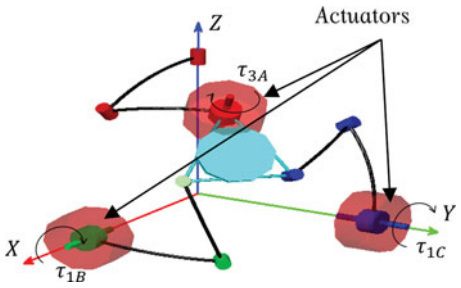


Fig. 18. Control mode 2 for singular configurations.

$\left[\tau_{1A}\ \tau_{1B}\ \tau_{1C}\right]^{\mathrm{T}}$. The Jacobian matrix is a 3×3 matrix and it corresponds to the non-redundant SPM. Its expression is presented in Eq. (3).

2. Control mode 2
   For the singular configuration mode, the actuators on the axes $\mathbf{Z}_{3A}$, $\mathbf{Z}_{1B}$, and $\mathbf{Z}_{1C}$ are active while the actuator on the axis $\mathbf{Z}_{1A}$ is passive. The SPM is equivalent to the one in Fig. 18. In this case, the provided torque vector τ is equal to $\left[\tau_{3A}\ \tau_{1B}\ \tau_{1C}\right]^{\mathrm{T}}$.
   In this case, the Jacobian matrices **A** and **B** are defined as follows:

$$\mathbf{A} = \left[\mathbf{Z_{1A}} \times \mathbf{Z_{2A}} \quad \mathbf{Z_{3B}} \times \mathbf{Z_{2B}} \quad \mathbf{Z_{3C}} \times \mathbf{Z_{2C}}\right]^{\mathbf{T}}, \tag{31}$$

$$\mathbf{B} = \mathbf{diag}[\boldsymbol{Z}_{3A}(\boldsymbol{Z}_{1A} \times \boldsymbol{Z}_{2A}) \quad \cdots \quad \boldsymbol{Z}_{1B}(\boldsymbol{Z}_{2B} \times \boldsymbol{Z}_{3B}) \quad \boldsymbol{Z}_{1c}(\boldsymbol{Z}_{2c} \times \boldsymbol{Z}_{3c})\ ]. \tag{32}$$

3. SimMechanics validation
   In order to validate the new structure and its control strategy before constructing the real device, we developed a SimMechanics model of the redundant SPM presented in Fig. 19.

The model is built using library blocks of SimMechanics package. The green blocks correspond to the nine revolute joints of the SPM. The base of the SPM corresponds to the blue block while the red block describes the end-effector. The actuated joints are defined by the axes $\mathbf{Z}_{1A}$, $\mathbf{Z}_{1B}$, and $\mathbf{Z}_{1C}$ for control mode 1 and $\mathbf{Z}_{3A}$, $\mathbf{Z}_{1B}$, and $\mathbf{Z}_{1C}$ for control mode 2.

The inputs are the actuated joint angles and the end-effector external torque. The outputs are the torques of active joints.

Figure 20 shows the trajectory of the moving platform which is a sinusoidal self-rotation around the singular configuration defined by $\varphi = 50^\circ$ and tilt angles defined by $\psi = 135^\circ$ and $\theta = 54^\circ$. This trajectory is chosen because it crosses many times the singular configurations. The torque applied on the end-effector is constant and equal to 1 N m along the x axis. The applied torque on the end-effector can be expressed by a vector as follows: $[100]^{\mathbf{T}}$.

The actuated joint of axes $\mathbf{Z}_{1A}$, $\mathbf{Z}_{1B}$, and $\mathbf{Z}_{1C}$ are equipped with dc motors with 70−m N m maximum torque and capstan reducers with a ratio of 16:1. So, the maximum joint torque is about 1.12 Nm.

The calculated joint torques for the classic SPM when the switching mode is not applied is shown on Fig. 21. It can be observed that when the SPM approaches the singular configuration the torques of all actuators increase and exceed the maximum torque value. Here, the torque limit, $\tau_{\max}$, is considered at 1 N m (Fig. 21) and not at the maximum actuator torque. This value has been adapted in order to ensure a safety margin and to reduce the risk of damage of dc motors as well. In this case, the control mode switches from mode 1 to mode 2.

When applying the switching control mode strategy, we obtain the joint torques of the redundant SPM presented in Fig. 22. We can see that for the two control modes the joint torques are lower than the maximum allowed torque (1 N m).

When applying alternatively mode 1 and mode 2, we can observe that in singularity area the torque of the actuator of axis $\mathbf{Z}_{1A}$ vanishes and the actuated torque of axis $\mathbf{Z}_{3A}$ remains within the torque limits. Moreover, the torques of the actuators of axes $\mathbf{Z}_{1B}$ and $\mathbf{Z}_{1C}$ also remain within the torque limits, instead of reaching infinite values as they would in the case of the non-redundant SPM.

https://doi.org/10.1017/S0263574714001751 Published online by Cambridge University Press

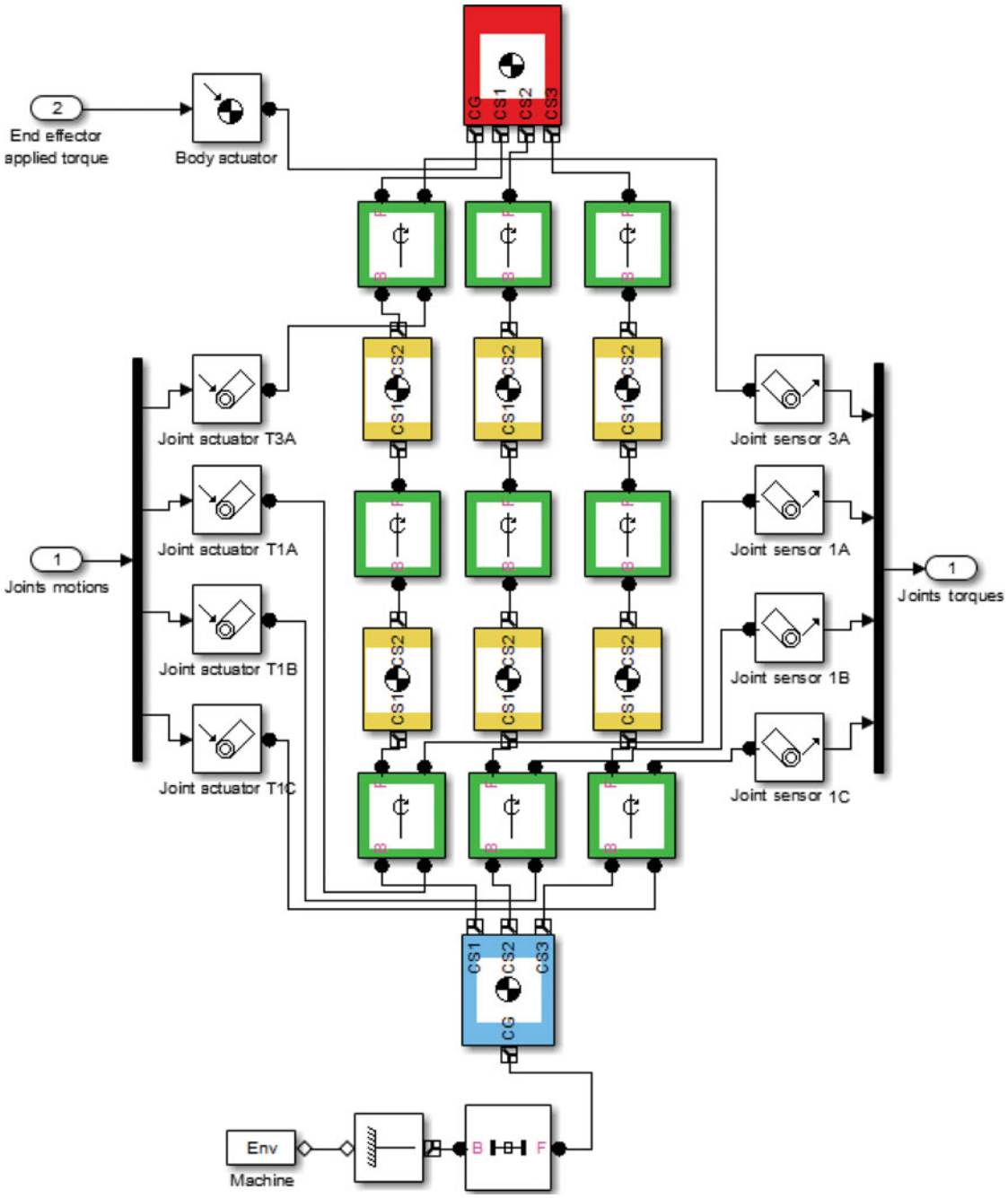


Fig. 19. The SimMechanics model of the redundant SPM.

6. Conclusions

This paper investigates a spherical parallel mechanism used as a haptic device for MIS applications. The presence of singularities inside the workspace alters the performances of the haptic device. As a consequence, the actuator torques increase highly near the singularity area and the FKM accuracy decreases. This work shows that the redundancy eliminates parallel singularity and improves the dexterity of the SPM. On the one hand a redundant sensor has been added to improve the accuracy of the FKM and to speed up the calculation time of the kinematic model. On the other hand, a redundant actuator has been used to keep the actuated torques within bounds. A control strategy for the new redundant SPM has been presented and tested using a SimMechanics model. This strategy uses a switching mode algorithm alternating a singular configuration mode and a singularity-free mode. This algorithm has been successfully tested in an experimental simulation showing that the redundancy

https://doi.org/10.1017/S0263574714001751 Published online by Cambridge University Press

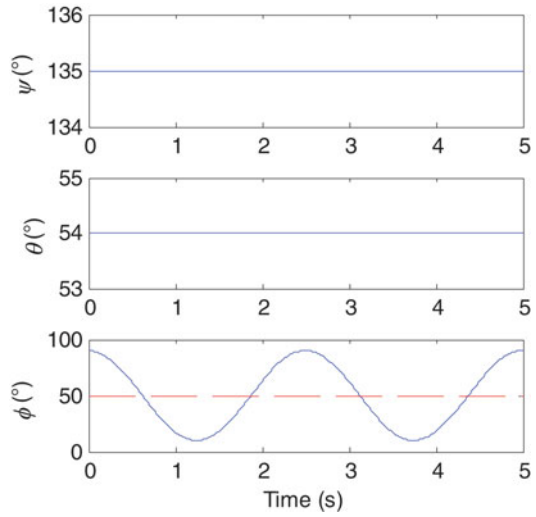


Fig. 20. The trajectory of the SPM end-effector.

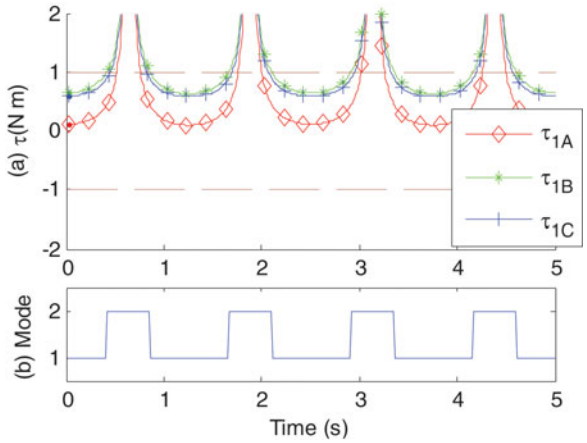


Fig. 21. (a) Calculated joint torques for the classic SPM; (b) control mode.

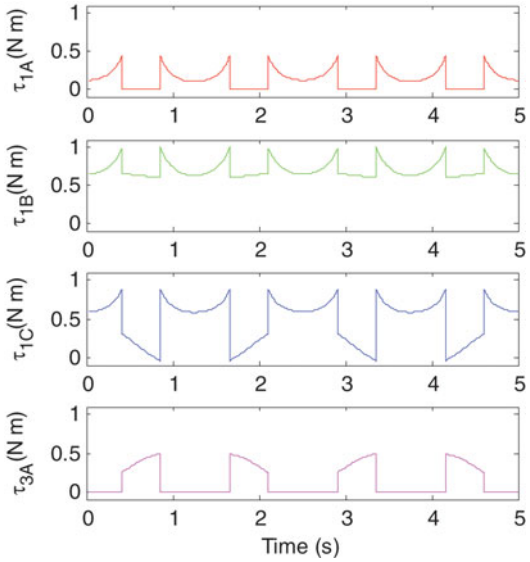


Fig. 22. Calculated joint torques of the redundant SPM.

https://doi.org/10.1017/S0263574714001751 Published online by Cambridge University Press

greatly improves the mechanism performance throughout the workspace and eliminates the parallel singularity effects.

Acknowledgements
This research is supported by the "Poitou-Charentes" region 2007–2013 (program project 10 images and interactivities), in partnership with the European Union (FEDER/ERDF, European Regional Development Fund). This research is supported by ROBOTEX, the French national network of robotics platforms (No. ANR-10-EQPX-44-01).

References

1. H. P. Jaydeep, "Robotic assisted minimally invasive surgery," *J. Minim. Access Surg.* **5**(1), 1–7 (2009).
2. P. Gomes, 2011, "Surgical robotics: reviewing the past, analysing the present, imagining the future," *Robot. Comput.-Integr. Manuf.* **27**(2), 261–266.
3. D. Chablat and P. Wenger, "Architecture optimization of a 3-DOF parallel mechanism for machining applications, the orthoglide," *IEEE Trans. Robot. Autom.* **19**(3), 403–410 (2003).
4. M. Arsenault and R. Boudreau, "The synthesis of three-degree-of-freedom planar parallel mechanisms with revolute joints (3-RRR) for an optimal singularity free workspace," *J. Robot. Syst.* **21**(5), 259–274 (2004).
5. L. Birglen, C. Gosselin, N. Pouliot, B. Monsarrat and T. Laliberte, "SHaDe, a new 3-DOF haptic device," *Robot. Autom.* **18**(2), 166–175 (2002).
6. J. Wu, J. Wang, L. Wang and T. Li, "Dynamic model and force control of the redundantly actuated parallel manipulator of a 5-DOF hybrid machine tool," *Robotica* **27**(1), 59–65 (Jan. 2009).
7. E. Tatlicioglu, D. Braganza, T. C. Burg and D. M. Dawson, "Adaptive control of redundant robot manipulators with sub-task objectives," *Robotica* **27**, 873–881 (2009).
8. H. Sadeghian, L. Villani, M. Keshmiri and B. Siciliano, "Dynamic multi-priority control in redundant robotic systems," *Robotica* **31**, 1155–1167 (2013).
9. A. Zubizarreta, I. Cabanes, M. Marcos and C. Pinto, "A redundant dynamic model of parallel robots for model-based control," *Robotica* **31**, 203–216 (2013).
10. M. Kroh *et al*., "First human surgery with a novel single-port robotic system: Cholecystectomy using the Da Vinci single-site platform," *Surg. Endosc.* **25**, 3566–3573 (2011).
11. A. A. Thakre, "Is smaller workspace a limitation for robot performance in laparoscopy?," *J. Urol.* **179**, 1138–1143 (2008).
12. M. A. Laribi, T. Rivière, M. Arsicault and S. Zeghloul, "A Design of Slave Surgical Robot Based on Motion Capture," *Proceedings of the 2012 IEEE International Conference on Robotics and Biomimetics*, Guangzhou, China (Dec. 11–14, 2012) pp. 600–605.
13. A. Chaker, M. A. Laribi, S. Zeghloul and L. Romdhane, "Design and optimization of spherical parallel manipulator as a haptic medical device," *Proceedings of the 37th Annual Conference of the IEEE Industrial Electronics Society, focusing on industrial and manufacturing theory and applications of electronics, controls, communications, instrumentation and computational intelligence*, Melbourne, Australia (Nov. 7–10, 2011) pp. 80–85.
14. A. Chaker, A. Mlika, M. A. Laribi, L. Romdhane and S. Zeghoul, "Synthesis of a spherical parallel manipulator for a dexterous medical task," *Front. Mech. Eng.* **7**(2), 150–162 (2012).
15. S. Zeghloul and J. A. Pamanes, "Multi criteria optimal placement of robots inconstrained environments," *Robotica* **11**(1), 105–110 (1993).
16. S. Zeghloul, "Développement d'un système de CAO-Robotique intégrant la planification de trajectoires et la synthèse de sites robotisés," State Phd, Poitiers, 14 février 1991.
17. S. Leguay-Durand and C. Reboulet, "Optimal design of a redundant spherical parallel manipulator," *Robotica* **15**, 399–405 (1997).
18. M. Ceccarelli, G. Carbone and E. Ottaviano, "Multi criteria optimum design of manipulators," *Bull. Pol. Acad. Sci., Tech. Sci.* **53**(1), 9–18 (2005).
19. Z. Gao, D. Zhang, X. Hu and Y. Ge, "Design, analysis, and stiffness optimization of a three degree of freedom parallel manipulator," *Robotica* **28**, 349–357 (2010).
20. C. Gosselin and J.-P. Merlet, "The direct kinematics of planar parallel manipulators: special architectures and number of solutions," *Mech. Mach. Theory* **29**, 1083–1097 (1994).
21. J.-P. Merlet, "Direct kinematics of parallel manipulators," *IEEE Trans. Robot. Autom.* **9**(6), 842–845 (1993).
22. L. Baron and J. Angeles, "The direct kinematics of parallel manipulators under joint-sensor redundancy," *IEEE Trans. Robot. Autom.* **16**(1), (2000).
23. E. Celaya, "Interval propagation for solving parallel spherical mechanisms," **In**: *Advances in Robot Kinematics* (J. Lenarcic and F. Thomas, eds.) (Kluwer Academic Publishers, 2002) pp. 415–422.
24. C. M. Gosselin, J. Sefrioui and M. J. Richard, "On the direct kinematics of spherical three-degree-of-freedom parallel manipulators of general architecture," *ASME J. Mech. Des.* **116**(2), 594–598 (1994).
25. S. Bai, M. R. Hansen and J. Angeles, "A robust forward displacement analysis of spherical parallel robots," *Mech. Mach. Theory* **44**(12), 2204–2216 (2009).

https://doi.org/10.1017/S0263574714001751 Published online by Cambridge University Press

26. H. Saafi, M. A. Laribi, S. Zeghloul and M. Y. Ibrahim, "Development of a Spherical Parallel Manipulator as a Haptic Device for a Tele-Operation System: Application to Robotic Surgery," *Proceedings of the 39th International Conference on Industrial Electronics Society*, Vienna, Austria (Nov. 10–13, 2013) pp. 4095–4100.
27. A. Chaker, A. Mlika, M. A. Laribi, L. Romdhane and S. Zeghloul, "Clearance and manufacturing errors' effects on the accuracy of the 3-RCC spherical parallel manipulator," *Eur. J. Mech. A* **37**, 86–95 (Jan.–Feb. 2013).
28. A. Maciejewski and C. A. K. Bein, "The singular value decomposition: Computation and applications to robotics," *Int. J. Robot. Res.* **8**, 63–79 (1989).

https://doi.org/10.1017/S0263574714001751 Published online by Cambridge University Press